Density Changes Accompanying Wave Propagation in the Cerium-Catalyzed Belousov−Zhabotinsky Reaction

Motohiro Kasuya,[†] Koji Hatanaka,[†] Jonathan Hobley,[†] Hiroshi Fukumura,*[,†] and Hana Sevcíkova[‡]

Department of Chemistry, Graduate School of Science, Tohoku University, Sendai, 980-8578, Japan, and Center of Nonlinear Dynamics of Chemical and Biological Systems, Prague Institute of Chemical Technology, Technicka 5, 166 28 Prague 6, Czech Republic

Received: September 5, 2004; In Final Form: December 9, 2004

Refractive index measurement using an interferometric imaging system and observation of chemical wave shapes were carried out during chemical wave propagation of a cerium-catalyzed Belousov−Zhabotinsky (BZ) reaction. Densities increased as chemical waves propagated in samples without NaBr, and decreased in samples with NaBr. Concentration changes of malonic acid, bromomalonic acid, and BrO_3^- were estimated from Raman spectral measurements in a stirred batch BZ reaction, and these also exhibited differences between samples with and without NaBr. It is proposed that a reaction subset yielding low molecular weight carboxylic acids is predominant in samples with NaBr, whereas a pathway leading to dibromoacetic acid or tribromoacetic acid production is the major process in samples without NaBr.

1. Introduction

Chemical waves are important examples of reaction−diffusion self-organized concentration structures because they provide good models to simulate the formation of space and time patterns in living systems.[1−4] It has been found that chemical wave propagation can be accompanied by hydrodynamic effects probably derived from density changes occurring in the solution.[5−11] In general, density changes can result from either temperature[7,11] and/or concentration changes[6−11] occurring during these chemical reactions.

Experimental studies[8−10] and theoretical discussions[6,7] on ferroin-catalyzed Belousov−Zhabotinsky (BZ) waves propagating in closed vessels have demonstrated that gravity effects on the density difference generated in solution can change both the wave shape and the propagation speed. Pojman and Epstein[7] have shown that the contribution of the temperature change to the density change in a BZ reaction is negligible in comparison with density changes resulting from the changes in species concentrations. They presume that the main contribution to the density change across the propagating wave results from the transformations between ferroin and ferriin. On the basis of tabulated data, they calculated the differences of partial molar volumes of Fe(II)/Fe(III) and $Fe(CN)_6^{3-}/Fe(CN)_6^{4-}$ redox couples and inferred that the change of the partial molar volumes during the oxidation of ferroin to ferriin is negative. As a consequence, the narrow region of the wave containing the oxidized form of the catalyst is denser than the reduced regions of the wave both in front of and behind the oxidized region. This density gradient should give rise to downward hydrodynamical flows that would distort the shape of ascending waves and would accelerate descending waves keeping their shape stable.

Pojman and Epstein's predictions were partly confirmed by experiments performed both in normal and in micro-gravity conditions.[9] Under the normal gravity conditions, the acceleration of descending and deceleration of ascending waves in the ferroin-catalyzed BZ reaction was found; however, no distortion of ascending waves was observed. Because these changes in the speed of propagation did not occur in a micro-gravity environment, it was concluded that there is the density gradient formed during the wave propagation invoking hydrodynamic flows in the normal gravity environment.

The propagation of ferroin-catalyzed BZ waves was studied in a horizontal capillary tube by Sevcíkova and Müller, both with and without the influence of d.c. electric fields.[8] Although no distortions of the wave were observed without the electric field, S-shape deformations of the waves were observed when a sufficiently large electric field was switched on with the negative electrode facing the approaching wave. Because the lower part of the wave preceded the upper part, it has been concluded that the oxidized region with ferriin is heavier than the reduced solution in front of the wave. This conclusion is in accord with the predictions made by Pojman and Epstein.

Large distortions of waves propagating upward in the cylindrical tube were observed by Menzinger et al. in the manganese-catalyzed BZ reaction.[10] Because the downward propagating waves were stable, their observation seems to prove Pojman and Epstein's assumption that there is an increase in the solution density when the reduced form of the catalyst becomes the oxidized form. On the other hand, measurements of the density changes in a stirred batch system of bubble-free manganese-catalyzed BZ reaction have shown that the density decreases in a stepwise manner with each oscillation. Despite the fact that all of these reports have implied density changes during BZ reactions, no one has yet directly measured in-situ density changes accompanying wave propagation.

In the current research, we constructed an instrument to measure refractive index changes using an interferometric imaging system to investigate density changes during chemical wave propagation. The employed method allows us to obtain a high precision estimate of the density in the sample solution, supposing, reasonably, that refractive index changes are accompanied by density changes. We have chosen the cerium-

* Corresponding author. Phone and fax: +81 22-217-6567. E-mail: fukumura@orgphys.chem.tohoku.ac.jp.
[†] Tohoku University.
[‡] Prague Institute of Chemical Technology.

10.1021/jp046001l CCC: $30.25
Published on Web 02/02/2005

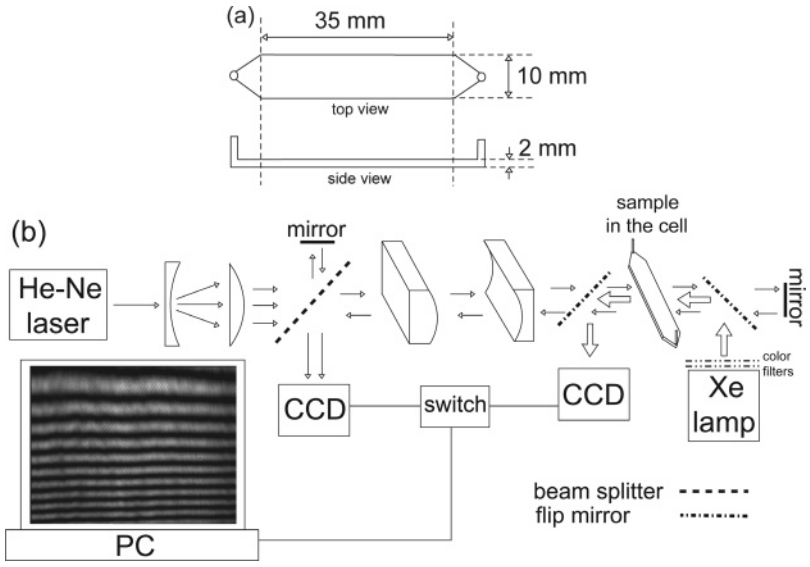

Figure 1. Experimental setup for observation of chemical wave shape: (a) the dimensions of the cell; and (b) the imaging system for simultaneous interferometry and absorbance measurements.

catalyzed system because cerium(IV) and (III) absorb light in the UV region only. On the contrary, ferroin and ferriin both have light absorption bands in the UV and visible regions, which would affect the measurements of refractive index changes when using visible light. There are reports on chemical waves in the cerium-catalyzed BZ reaction;[12,13] however, no report has been given on hydrodynamic effects during chemical wave propagation for this system. We also studied the effect of NaBr on density changes as well as chemical wave profiles propagating upward and downward in the cerium-catalyzed BZ reaction. This is because many studies on BZ reactions have been performed with different initial concentrations of bromide ion. It has been reported that the initial bromide concentration plays an important role in controlling the ferroin-catalyzed BZ reaction.[14] Interestingly, we have found that density changes during chemical wave propagation depended on the initial bromide concentration.

Raman spectral measurements were also performed to monitor changes in concentrations of some reaction species. Raman spectroscopy is a useful method for the direct observation of concentration changes of specific molecular species in an aqueous solution.[15] The presence of many kinds of carboxylic acids in the BZ reaction have been reported and their concentrations have been measured, in one report using ^{1}H NMR,[16] in another using high performance liquid chromatography (HPLC),[17] and in one using both techniques.[18] Unfortunately, ^{1}H NMR must be carried out in D_2O instead of H_2O, in which case the reaction kinetics are expected to be different. Further HPLC does not give a direct measurement of the real time BZ reaction and as such is complicated by the need for off-line measurement. Utilizing Raman spectroscopy for in-situ monitoring, we observed a decrease in the concentrations of malonic acid and BrO_3^- ion and an increase in the bromomalonic acid concentration regardless of whether NaBr was added to the reaction mixtures. On the basis of experimental results and the Marburg−Budapest−Missoula (MBM) mechanism,[17] we discuss the density change mechanism in connection with predominant reaction pathways involved in the BZ reaction.

2. Experimental Section

2.1. Reagents. H_2SO_4 (95%, Wako Chemicals), $NaBrO_3$, malonic acid (MA), and $Ce_2(SO_4)_3 \cdot 8H_2O$ (Nacalai Tesques), NaBr, and $Ce(SO_4)_2 \cdot 4H_2O$ (Kanto Kagaku Reagents) were reagent grade and used without any purification. Bromomalonic acid (BrMA) was prepared as described in the literature.[19] All solutions were prepared with distilled water.

The aqueous sample solutions for chemical wave observation and interferometric imaging were made as follows. NaBr, H_2SO_4, and $NaBrO_3$ aqueous solutions were mixed in a volumetric flask and became brown colored due to bromine generation. Malonic acid solution was added to this mixture, and the brown solution color faded within about 2 min due to bromination of malonic acid. $Ce(SO_4)_2$ solution and water were added to a final volume of 5 mL for the mixture. Two sample compositions were used, both having [MA] = 50 mM, $[H_2SO_4]$ = 150 mM, $[BrO_3^-]$ = 300 mM, $[Ce^{4+}]$ = 6 mM; however, in one composition, $[Br^-] = 10$ mM, and in the other, $[Br^-] = 0$ mM.

2.2. Observation of the Chemical Wave Shape. Profiles of chemical waves propagating downward and upward were observed with a conventional method as reported.[13] Light from a Xe lamp centered at 367 nm selected by color filters (UVD-36A, Toshiba) passed through the sample solution in a quartz glass cell of 2 mm × 10 mm × 35 mm dimensions as shown in Figure 1a. The profiles of chemical waves induced by a silver wire were imaged using a charge-coupled device (CCD) at 1 min intervals.

2.3. Interferometry. The refractive index change resulting from chemical wave propagation was measured with a Michelson interferometer as shown in Figure 1b. Light from a He−Ne laser (λ = 633 nm, 7 mW) was expanded to about 1 cm in diameter and divided into two beams by a beam splitter. One of the beams was reduced to 1 mm thickness by two cylindrical lenses and passed through the sample cell. This beam returned on the same path and was overlapped with the other beam on a CCD, creating an interferometric image. The sample cell for this measurement was the same as the one used in observation of chemical wave shape. The cell was imaged through the 2 mm window, giving an interaction path length of 10 mm.

An example of an interferometric image is shown in Figure 2a. Refractive index changes were obtained from the interferometric images. The light intensity profile I_x along the white line drawn in Figure 2a is shown in Figure 2b. In principle, the variation in I_x as a function of the position x is given by

$$I_x = I_0 + A \cdot \sin(\omega \cdot x + \phi) \quad (1)$$

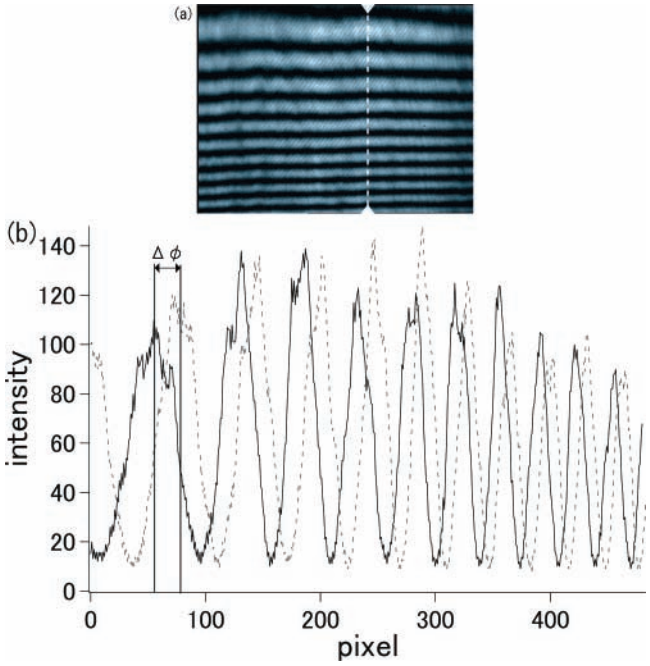

Figure 2. Interferometric image and the cross sections: (a) interferometric image before the reaction; (b) profiles of the light intensity along the white dashed line in (a). (−) Before chemical wave propagation, (- - - -) during the passage of a chemical wave.

where A and ϕ represent amplitude and phase, respectively. The parameter ω depends on optical path length differences between the reference and sampling beams, which is not essential in the measurement of refractive index changes in the sample solution.

Differential phase $\Delta\phi$ is the difference between ϕ from an image during chemical wave propagation and ϕ_0, which is the phase of the image taken before the reaction starts. The differential phase can be converted into the refractive index change Δn using eq 2:

$$\Delta n = \lambda \cdot \Delta\phi / 2\pi \cdot d \tag{2}$$

where d and λ are, respectively, the path length and the wavelength of the probe light ($d = 20$ mm and $\lambda = 633$ nm).

2.4. Absorbance Measurement. An absorbance measurement at 367 nm enabled us to monitor the Ce^{4+}/Ce^{3+} concentration, and this was performed at the same time as interferometry using the Xe lamp with color filters (15 nm bandwidth) and a CCD camera. The molar absorption coefficient of cerium(IV), $\epsilon_{Ce(IV)}$, at 367 nm is 1.01×10^3 L mol^{-1} cm^{-1}.

2.5. Density and Refractive Index Measurement. Measurements of densities and refractive indices of water solutions of various reaction components were performed to estimate the relationship between refractive index change and the solution density change. Densities were measured using a pycnometer (25 mL) and a precise balance (±0.0005 g). These measurements were performed at 290.7 ± 0.2 K.

The refractive index of a solution was measured with a conventional method[20] by using a prismatic cell. A light beam emitted from a He−Ne laser passed through the cell filled with a sample solution and was guided to the screen of a CCD camera. The displacement (Δd) of the light beam was obtained from a shift of the maximum light intensity pixel of the CCD camera. This refractometer was calibrated in the following way. Values of Δd were measured using various concentrations of ethanol/water mixtures. Composition and refractive indices in the literature[21] were found to have a linear relation in the region less than 15 wt %. We can calculate a refractive index using the following equation:

$$n_{\text{ethanol}} = 6.59 \times 10^{-4} \times \text{wt \%(ethanol)} + 1.33320 \tag{3}$$

The relationship between Δd and refractive indices was linear, and the measured Δd can be transformed to a refractive index change, Δn, by the empirically derived equation:

$$\Delta n = 2.378 \times 10^{-5} \cdot \Delta d \tag{4}$$

The detection limit of the refractive index change using this system was 2×10^{-6}.

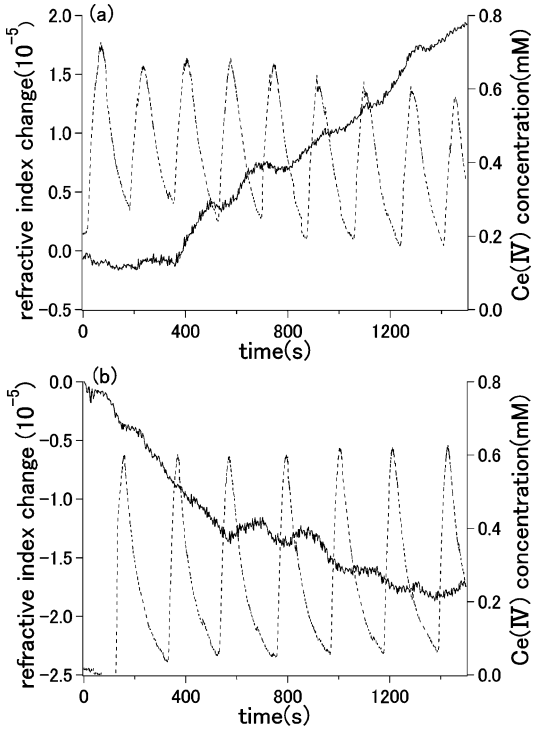

Figure 3. Refractive index (−) and Ce^{4+} concentration changes (- - - -) during chemical wave propagation: (a) in the sample without NaBr; and (b) in the sample with NaBr.

2.6. Raman Spectral Measurement. Raman spectra of the sample solution were measured in a 1 cm path length conventional quartz cell with a magnetic stirrer. The second harmonic of a Nd:YAG laser ($\lambda = 532$ nm, Quantel, Brilliant) was used as the light source. The scattered light was collected at 90° to the laser beam propagation and was analyzed using a multichannel analyzer with an image intensifier (Hamamatsu Photonics PMA-50). The reaction was initiated by injecting a $Ce(SO_4)_2$ solution into an aqueous mixture of MA, H_2SO_4, $NaBrO_3$, and NaBr. The initial concentrations were the same as for the chemical wave observation experiment. Raman spectra were integrated over 300 s, which means that we monitored the long-term changes rather than the oscillatory changes of reaction components. Simultaneously in the same quartz cell, the cerium(IV) concentration was monitored as described in section 2.4. The temporal response of the absorbance measurement was quick enough to monitor the oscillatory cerium redox reaction in the cell.

3. Results and Discussions

3.1. Refractive Index Changes during Chemical Wave Propagation. Refractive index changes during the wave propagation measured by interferometric imaging techniques are shown in Figure 3. The time scale in the figure only relates to

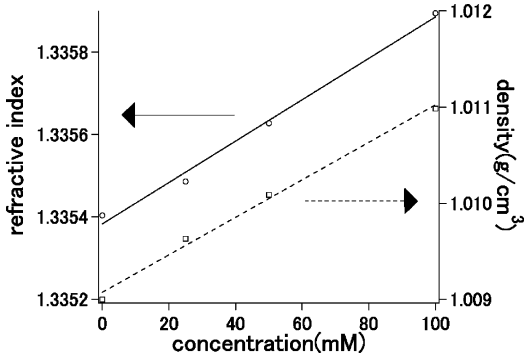

Figure 4. Refractive index (− and ○) and density (- - - - and □) versus concentration for MA.

the start of the measurement; the time 0 is the moment when the first wave appeared in the monitored region. This is because the actual time between stimulation by the silver wire and observation of the first propagating wave in the monitored region varied with the concentration of NaBr. The refractive index increased in a stepwise manner in the sample without NaBr by $+3.2 \times 10^{-6}$ per wave during the propagation of six waves from 350 to 1410 s as can be seen in Figure 3a. On the other hand, the refractive index decreased in the sample with NaBr by -2.5×10^{-6} per wave during the propagation of six waves from 120 to 1390 s as shown in Figure 3b. Assuming that it was a density change that was responsible for the refractive index change, the density increased in the sample without NaBr and decreased in the sample with NaBr.

3.2. Light Absorption Changes during Chemical Wave Propagation. Concurrent measurements of light absorption indicated that the cerium(IV) concentration oscillated during wave propagation with almost the same period as was observed for the period of the stepwise change in refractive index. Notably, the overall refractive index changes in the sample with and without NaBr were opposite to each other. Because the amount of NaBr is critical in the formation of various bromocarboxylic acids,[14] we consider that these compounds may play an important role in the refractive index change.

3.3. Partial Molar Refractive Indices and Densities of BZ Reaction Components. The relationship between the MA concentration and either density or refractive index was linear in aqueous solution as shown in Figure 4. The dependence of the refractive indices and densities of solutions of NaBr, BrMA, $NaBrO_3$, $Ce(SO_4)_2$, and $Ce_2(SO_4)_3$ in 0.15 M H_2SO_4 upon the components' concentrations also followed linear relationships. Thus, partial molar refractive index, n_i, and partial molar density, ρ_i, could be obtained from the slopes of these graphs, and these are listed in Table 1.

The refractive index and density ratio ρ_i/n_i, obtained from the data in Table 1, were used for the conversion of refractive index to density. The maximum value of ρ_i/n_i was 7.05 g cm^{-3} for $NaBrO_3$, and the minimum value was 3.51 g cm^{-3} for MA. On the basis of the range of ρ_i/n_i in Table 1, we assume, in the following discussion, that a value 5.3 g cm^{-3} can be used as a typical average value of the refractive index and density ratio. The refractive index changes were converted to density changes using the averaged ratio value. In the sample without NaBr, the density change per wave propagating at a given point is $+1.7 \times 10^{-5}$ g cm^{-3} (± 0.6 g cm^{-3}), while the change in the sample with NaBr is -1.3×10^{-5} g cm^{-3} (± 0.5 g cm^{-3}).

3.4. Chemical Wave Shape during Ascending and Descending Propagation. Typical profiles of chemical waves in the BZ reaction both ascending and descending are illustrated in Figure 5. In the sample without NaBr, ascending waves (Figure 5a) propagated concentrically and slowly became flatter

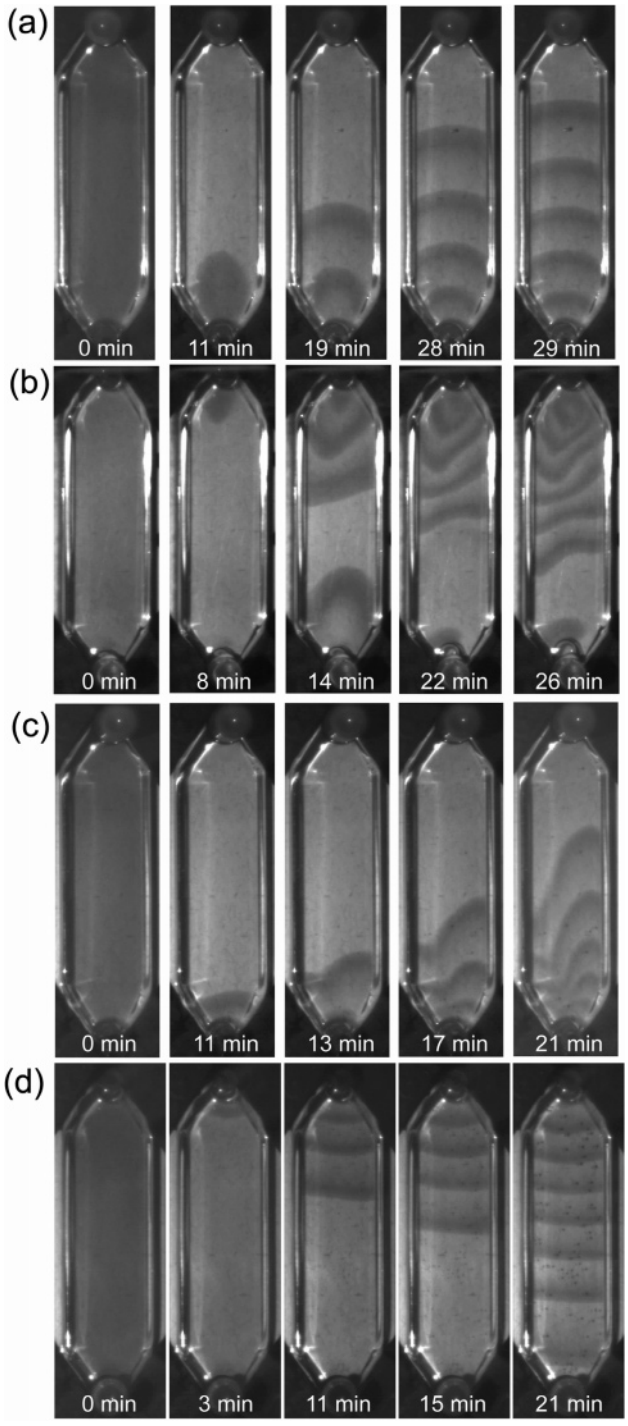

Figure 5. Chemical wave shape changes during cerium-catalyzed BZ reactions: (a) upward and (b) downward propagation using the sample without NaBr; (c) upward and (d) downward propagation using the sample with NaBr.

TABLE 1: Partial Molar Refractive Indices and Densities of BZ Reaction Components

component	n_i	ρ_i	ρ_i/n_i
H_2SO_4	0.01469	0.06840	4.66
NaBr	0.01784	0.08268	4.64
MA	0.005129	0.01802	3.51
BrMA	0.03708	0.2115	5.70
$NaBrO_3$	0.009851	0.06946	7.05
Ce^{4+}	0.05477	0.3104	5.67
Ce^{3+}	0.08210	0.3279	3.99
Na_2SO_4	0.001828	0.1091	5.97

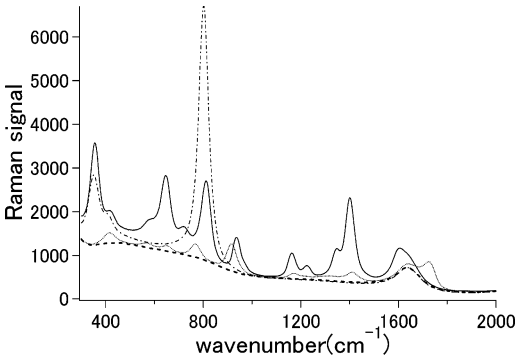

Figure 6. Raman spectra of 1 M BrMA (−), 1 M MA (····), 1 M BrO_3^- (− · −), and water (- - - -).

and flatter, while descending waves propagated inverse parabolically, later becoming parabolic in shape (Figure 5b). Inverse behavior to this was observed in the sample with 10 mM NaBr. Ascending waves (Figure 5c) propagated parabolically becoming inverse parabolic, while descending waves propagated concentrically becoming flatter (Figure 5d). The fact that ascending waves were stable and descending ones unstable in the sample without NaBr suggests that the density of the solution behind the wave is higher than the density of the solution in front of the wave. An opposite density change was considered to occur in the sample with 10 mM NaBr, because the descending waves were stable and ascending ones were unstable. The proposed density changes here are in agreement with the experimental results obtained by the refractive index measurements in section 3.1. Therefore, we can conclude that the density change would be responsible for the stability of wave propagation in the vertical cell.

It should be noted that tiny bubbles measuring around a few hundred micrometers were sometimes observed at the surface of the vertical cell during the observation of wave propagation. These bubbles appeared at the late stage and were more conspicuous in the sample with NaBr than the one without NaBr (for example, small dots in Figure 5d). The bubbles may consist of CO_2, because it is reported that the oxidation of MA and BrMA by Ce^{4+} leads to CO_2 generation.[22] This suggests that CO_2 generation was greater in the sample with NaBr than in the sample without NaBr. We will return to this point in section 3.6.

3.5. Long-Term Concentration Changes Monitored with Raman Spectroscopy. Figure 6 displays the Raman spectra of MA, BrMA, and $NaBrO_3$ aqueous solutions and that of water in the 300−2000 cm^{-1} region. Water's Raman spectrum has a peak at 1635 cm^{-1} and some peaks in the 300−900 cm^{-1} region.[23] $NaBrO_3$ solution has Raman peaks at 365, 421, and 805 cm^{-1}, which can be assigned to the Br−O bond.[24] The 780−830 cm^{-1} region containing the strongest peak is the best one to monitor the concentration of BrO_3^-. MA and BrMA had several peaks between the 300−1000 and the 1100−1800 cm^{-1} regions. It is expected that the intensity of the Raman signal from water is highly pH sensitive because of structural changes in water clusters. Therefore, the 400−900 and 1550−1700 cm^{-1} regions were not considered suitable for monitoring small spectral changes within these groups of small peaks. The Raman signal in the region 1330−1450 cm^{-1} was used to monitor the BrMA concentration, because the only other peaks in this region were weak MA bands. Because the MA peak had a stronger signal than that of BrMA only in the region from 900 to 920 cm^{-1}, this spectral window was used for monitoring the MA concentration. The integrated intensities in these regions were normalized to the integrated intensity at 1040−1090 cm^{-1} to

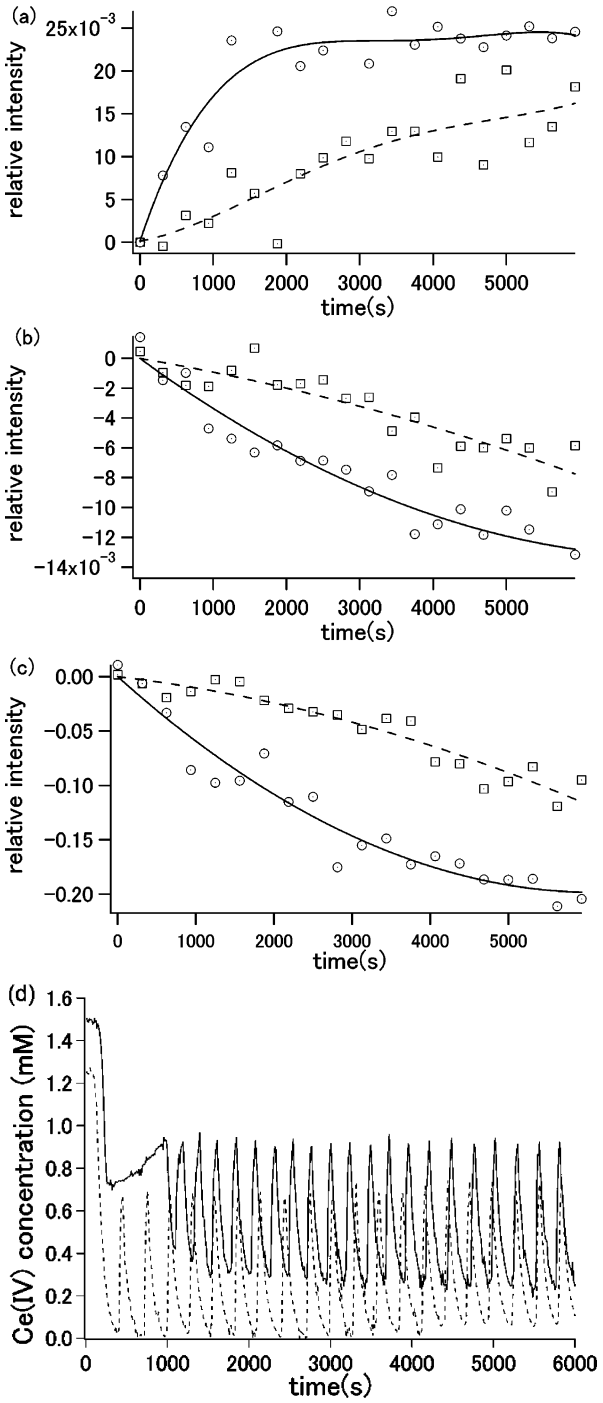

Figure 7. Integrated Raman spectral intensity and Ce^{4+} concentration changes in the sample with NaBr (- - - -) and without NaBr (−): (a) BrMA, (b) MA, (c) BrO_3^-, and (d) Ce^{4+}.

account for small spectra to spectra intensity variation. This region is the best one for normalization because it contains no peaks except for that of SO_4^{2-}, which should have a constant concentration during the reaction.

The changes in the Raman integrated intensity for BrO_3^-, MA, and BrMA and the absorbance changes of Ce(IV) during the course of the reaction in the stirred batch vessel are shown in Figure 7. The Ce(IV) absorbance in the sample without NaBr shows that the oscillations started after the long initial period of the excited state from 250 to 1000 s. From Raman spectroscopic data for the same sample, the concentration of BrMA increased rapidly from the beginning of the reaction until 1000 s, then more slowly until 2000 s, and finally it reached an

almost constant concentration at times longer than 3000 s. Concentrations of BrO_3^- and MA always decreased, and the rates of consumption of these species decelerated with time. On the other hand, in the sample with NaBr, the absorbance oscillated constantly from 250 s. The concentration of BrMA always increased and BrO_3^- and MA always decreased as the consumption rates accelerated with time. The extent of consumption of BrO_3^- and MA concentrations in the sample without NaBr was twice as large as that in the sample with NaBr from the reaction start until 6000 s.

3.6. Possible Mechanisms of Density Changes. Hegedus et al. suggested the Marburg−Budapest−Missoula (MBM) model, which can explain the reaction of many kinds of carboxylic and bromocarboxylic compounds based on their concentration as determined by HPLC.[17] This model involves many chemical components which can be responsible for changes in solution density accompanying wave propagation. Because we found that the BrMA concentration increased both with and without NaBr, as shown in Figure 7a, we did not include [BrMA] changes as a possible cause of density changes. When NaBr was not added, the concentration of BrMA increased markedly at the beginning of the reaction; however, the oscillation of Ce ions started just after the marked increase as shown in Figure 7d. This also suggests that density changes would not be due to BrMA.

The MBM model involves reactions of malonyl or bromomalonyl radical formed in the reaction with Ce^{4+}. It is proposed that these radicals react with $BrO_2\cdot$, giving rise to low molecular weight carboxylic acids as, for example, either mesoxalic acid (MOA) or oxalic acid (OA), finally forming CO_2. For example,

$$BrMA\cdot + \cdot BrO_2 \rightarrow BrMABrO_2$$

$$BrMABrO_2 \rightarrow OA + HOBr + Br^- + CO_2 + H^+$$

$$MA\cdot + \cdot BrO_2 \rightarrow MABrO_2$$

$$MABrO_2 \rightarrow MOA + HOBr$$

$$MOA + Ce^{4+} + H_2O \rightarrow OA + Ce^{3+} + COOH\cdot + H^+$$

$$OA + Ce^{4+} \rightarrow Ce^{3+} + COOH\cdot + CO_2 + H^+$$

$$COOH\cdot + Ce^{4+} \rightarrow Ce^{3+} + CO_2 + H^+$$

If these reactions are predominant, then acid components having relatively high densities, as compared to other chemical components, would be removed from the solution by decomposing into CO_2, leading to a reduction in solution density. This may be the case in our experiment with NaBr because the density of the sample decreased with wave propagation. Actually, we found that bubble formation, which was probably due to CO_2 generation during wave propagation, was more prominent in the sample with NaBr than in the sample without NaBr.

There may be other reactions in the MBM model that result in increases in solution density with wave propagation. For instance, MA is brominated to BrMA, and BrMA is further brominated to dibromomalonic acid (Br_2MA) as follows.

$$BrMA(enol) + Br_2 \rightarrow Br_2MA + Br^- + H^+$$

$$BrMA(enol) + HOBr \rightarrow Br_2MA + H_2O$$

Although Br_2MA was not directly detected with HPLC analysis, dibromoacetic acid was confirmed to increase as the end product in the Ce-catalyzed batch reaction.[17] The concentration of bromoethenetricarboxilic acid was also found to increase constantly during the reaction. If these processes yielding high density components are predominant, the solution density would increase, which can probably explain density increases with wave propagation in the experiment without NaBr.

4. Conclusion

Based on refractive index changes measured by the interferometric imaging system, the density is considered to increase in the sample without NaBr and decrease in the sample with NaBr. Concentration changes of BrMA, MA, and BrO_3^- were monitored in stirred sample solutions with Raman spectroscopy. Comparing the MBM model with our experimental results, we propose that the formation of low molecular weight carboxylic acids would be predominant in the sample with NaBr, whereas the reaction yielding high molecular weight carboxylic acids would be a major process in the sample without NaBr.

Acknowledgment. Funding for this work has been partly provided by a Grant-in-Aid from the Ministry of Education, Science, Sports, and Culture of Japan (13440204, 14740318, 16072203), and by Research Project No. MSM 223400007 from the Ministry of Education of the Czech Republic.

References and Notes

(1) Field, R. J.; Burger, M. *Oscillations and Traveling Waves in Chemical Systems*; Wiley: New York, 1985.
(2) Kapral, R.; Showalter, K. *Chemical Waves and Patterns*; Kluwar Academic Publishers: Dordrecht, 1995.
(3) Turing, A. M. *Philos. Trans. R. Soc. London* **1952**, *B237*, 37.
(4) Kondo, S.; Asai, R. *Nature* **1995**, *376*, 765.
(5) Rodriguez, J.; Vidal, C. *J. Phys. Chem.* **1989**, *93*, 2737.
(6) Wu, Y.; Vasquez, D. A.; Edwards, B. F.; Wilder, J. W. *Phys. Rev. E* **1995**, *51*, 1119.
(7) Pojman, J. A.; Epstein, I. R. *J. Phys. Chem.* **1990**, *94*, 4966.
(8) Sevcikova, H.; Müller, S. C. *Phys. Rev. E* **1999**, *60*, 532.
(9) Fujieda, S.; Mogami, Y.; Furuya, A.; Zhang, W.; Arashio, T. *J. Phys. Chem.* **1997**, *101*, 7926.
(10) Menzinger, M.; Tzalmona, A.; Armstrong, R. L.; Cross, A.; Lemaire, C. *J. Phys. Chem.* **1992**, *96*, 4725.
(11) Komlosi, A.; Nagy, I. P.; Bazsa, G.; Pojman, J. A. *J. Phys. Chem. A* **1998**, *102*, 9136.
(12) Nagy-Ungvarai, Z.; Tyson, J. J.; Hess, B. *J. Phys. Chem.* **1989**, *93*, 707.
(13) Nagy-Ungvarai, Z.; Müller, S. C.; Tyson, J. J.; Hess, B. *J. Phys. Chem.* **1989**, *93*, 2760.
(14) Li, H.; Huang, X. *Chem. Phys. Lett.* **1996**, *255*, 137.
(15) Hobley, J.; Kajimoto, S.; Takamizawa, A.; Ohta, K.; Tran-Cong, Q.; Fukumura, H. *J. Phys. Chem. B* **2003**, *107*, 11418.
(16) Ruoff, P.; Hansen, E. W.; Noyes, R. M. *J. Phys. Chem.* **1987**, *91*, 3393.
(17) Hegedus, L.; Wittmann, M.; Noszticzius, Z.; Yan, S.; Sirimungkala, A.; Försterling, H.-D.; Field, R. J. *Faraday Discuss.* **2001**, *120*, 21.
(18) Sirimungkala, A.; Försterling, H.-D.; Noszticzius, Z. *J. Phys. Chem.* **1996**, *100*, 3051.
(19) Försterling, H.-D.; Stuk, L. *J. Phys. Chem.* **1991**, *95*, 7320.
(20) Kingslake, R. *Applied Optics and Optical Engineer Volume IV*; Academic Press: New York, 1967.
(21) Washburn, E. W. *International critical tables of numerical data, physics, chemistry and technology*; McGraw-Hill: New York, 1929.
(22) Nagygyory, S.; Wittmann, M.; Pinter, S.; Visegrady, A.; Dancso, A.; Noszticzius, Z.; Hegedus, L.; Försterling, H.-D. *J. Phys. Chem.* **1999**, *103*, 4885.
(23) Carey, D. M.; Korenowski, G. M. *J. Chem. Phys*. **1998**, *108*, 2669.
(24) Shen, S. T.; Yao, Y. T.; Wu, T. *Phys Rev.* **1937**, *51*, 235.